PHYSICAL REVIEW B **95**, 035152 (2017)

Electronic structure of self-doped layered $Eu_3F_4Bi_2S_4$ material revealed by x-ray absorption spectroscopy and photoelectron spectromicroscopy

E. Paris,[1] T. Sugimoto,[1,2,3] T. Wakita,[4] A. Barinov,[5] K. Terashima,[4] V. Kandyba,[5] O. Proux,[6] J. Kajitani,[7] R. Higashinaka,[7] T. D. Matsuda,[7] Y. Aoki,[7] T. Yokoya,[4] T. Mizokawa,[8] and N. L. Saini[1]

[1]*Dipartimento di Fisica, Universitá di Roma "La Sapienza" - P. le Aldo Moro 2, 00185 Roma, Italy*
[2]*Department of Complexity Science and Engineering, University of Tokyo, 5-1-5 Kashiwa 277-8561, Japan*
[3]*Institute for Solid State Physics, University of Tokyo, 5-1-5 Kashiwa 277-8561, Japan*
[4]*Research Institute for Interdisciplinary Science, Okayama University, Okayama 700-8530, Japan*
[5]*Elettra Sincrotrone Trieste S.C.p.A., Area Science Park, 34012 Basovizza, Trieste, Italy*
[6]*Observatoire des Sciences de l'Univers de Grenoble, 38041 Grenoble, France*
[7]*Department of Physics, Tokyo Metropolitan University, Hachioji, Tokyo 192-0397, Japan*
[8]*Waseda University, Department of Applied Physics, Tokyo 169-8555, Japan*

(Received 25 October 2016; revised manuscript received 6 December 2016; published 30 January 2017)

We have studied the electronic structure of $Eu_3F_4Bi_2S_4$ using a combination of Eu L_3-edge x-ray absorption spectroscopy (XAS) and space-resolved angle-resolved photoemission spectroscopy (ARPES). From the Eu L_3-edge XAS, we have found that the Eu in this system is in mixed valence state with coexistence of Eu^{2+}/Eu^{3+}. The bulk charge doping was estimated to be ∼0.3 per Bi site in $Eu_3F_4Bi_2S_4$, which corresponds to the nominal x in a typical $REO_{1-x}F_xBiS_2$ system (*RE*: rare-earth elements). From the space-resolved ARPES, we have ruled out the possibility of any microscale phase separation of Eu valence in the system. Using a microfocused beam we have observed the band structure as well as the Fermi surface that appeared similar to other compounds of this family with disconnected rectangular electronlike pockets around the X point. The Luttinger volume analysis gives the effective carrier to be 0.23 electrons per Bi site in $Eu_3F_4Bi_2S_4$, indicating that the system is likely to be in the underdoped region of its superconducting phase diagram.

DOI: 10.1103/PhysRevB.95.035152

The BiS_2-based superconductors are composed of a layered structure with active BiS_2 bilayers intercalated by insulating spacer layers [1]. The typical BiS_2-based system $REOBiS_2$ (*RE*: rare-earth elements) is usually a band insulator, and the band filling can be controlled by electron doping; by substituting O by F [2] or tetravalent ions by trivalent La at *RE* site [3]. As the doping level increases, superconductivity develops within the BiS_2 layers with the maximum T_c of 10.5 K found in $LaO_{0.5}F_{0.5}BiS_2$ [4]. The conduction bands are composed of Bi $6p_{x/y}$ orbitals giving rise to rectangular electron pockets around the X point of the Brillouin zone [5,6].

With the same crystal structure, $EuFBiS_2$ shows superconductivity without any doping. It is thought to be caused by the self-doped electrons coming from Eu that is in a mixed valence state with coexisting Eu^{2+} and Eu^{3+} [7]. A similar situation seems to occur in a new class of the BiS_2-based family $Eu_3F_4Bi_2S_4$ system that is found to show bulk superconductivity with $T_c = 1.5$ K induced by self-doping [8]. The structure is rather complex with an additional EuF_2 layer intercalated into the $EuFBiS_2$ structure as shown in Fig. 1(a).

In this work we have studied the electronic structure of $Eu_3F_4Bi_2S_4$ by means of Eu L_3-edge x-ray absorption spectroscopy (XAS) and space-resolved angle-resolved photoemission spectroscopy (ARPES); the Eu L_3-edge XAS is a bulk sensitive probe on the valence state while the space-resolved ARPES can reveal the space-dependent electronic structure, which is especially important on the present system with a mixed valence of Eu and highly disordered local symmetry [9–11].

High-quality single crystals of $Eu_3F_4Bi_2S_4$ were grown by the CsCl-flux method with powders of EuS, Bi_2S_3, and BiF_3. The excess CsCl flux was removed using H_2O. The crystals were well characterized for their crystal structures and transport properties prior to the spectroscopy measurements [12].

The Eu L_3-edge XAS measurements have been performed at BM30B beamline of the European Synchrotron Radiation Facility. At the BM30B, the synchrotron radiation was monochromatized by a double crystal Si(220) monochromator, and the energy resolution is close to the intrinsic resolution of the Si crystals, i.e., around 0.35 eV at the Eu L_3 edge [13]. Two Si mirrors covered by a Rh layer allow us to avoid high energy photons (harmonics). The $Eu_3F_4Bi_2S_4$ crystals were mounted in a continuous flow He cryostat and XAS measurements were carried out in a partial fluorescence yield mode at a temperature of 21 K. The experimental geometry in sketched in the inset of Fig. 1(b) with the linearly polarized light falling at an angle of $\simeq 33^\circ$ with respect to the normal direction of the sample. This angle avoids the polarization effects and provides the angle-independent bulk spectrum. The Eu L_3-edge absorption spectrum was collected by detecting the Eu $L_{\alpha 1}$ fluorescence photons over a large solid angle using a multielement Ge detector. The obtained XAS spectrum was corrected for the self-absorption using the FLUO algorithm embedded in Athena software [14].

Space-resolved ARPES measurements have been performed at the Spectromicroscopy beamline, Elettra synchrotron facility, Trieste [15]. Incident photons of 74 eV were focused using a Schwarzschild optics down to a 500 × 500 nm^2 beam spot. For the present measurements the total energy resolution is about ∼100 meV while the angular resolution is $\leqslant 0.5^\circ$. The single crystals of $Eu_3F_4Bi_2S_4$ were cleaved and oriented *in situ* at 40 K under ultrahigh vacuum condition ($<10^{-10}$ mbar). All the measurements were carried

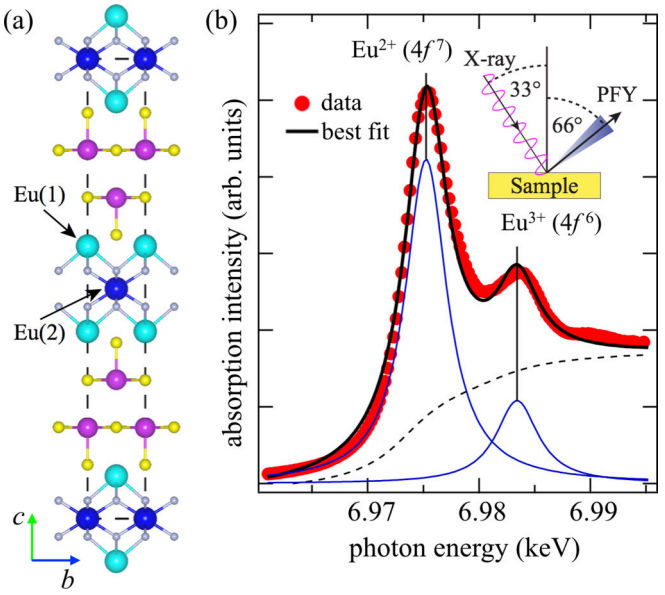

FIG. 1. (a) The crystal structure of $Eu_3F_4Bi_2S_4$ as obtained from structural refinement of Ref. [8], the two nonequivalent crystal sites for Eu are shown. (b) The Eu L_3-edge x-ray absorption spectrum (red bubbles) shown along with the best fit (black solid line) composed of two Lorentzian components (blue solid lines) plus the background function (dashed line). Inset shows a sketch of the fluorescence yield (PFY) detection geometry.

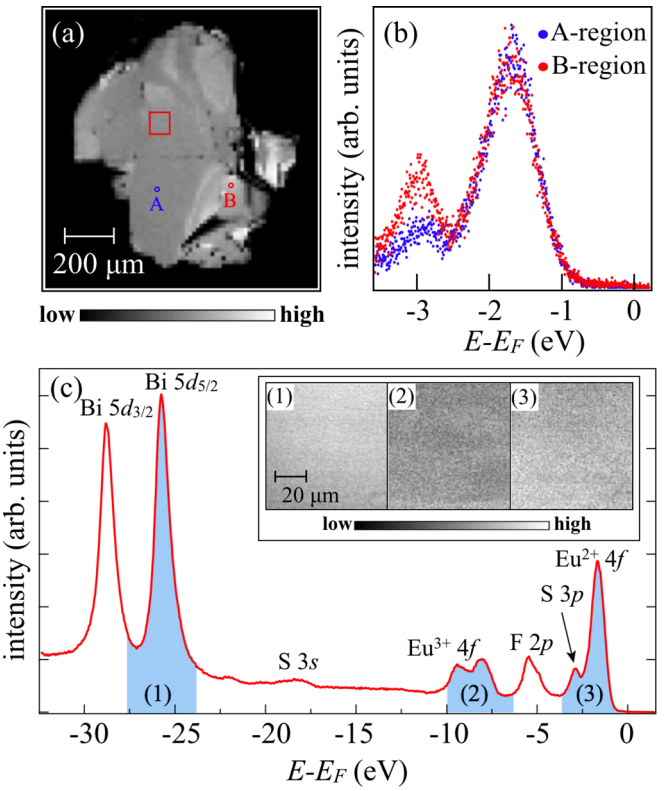

FIG. 2. (a) Photoelectron spectromicroscopy image of the cleaved single crystal of $Eu_3F_4Bi_2S_4$. The photoemission intensity is integrated from -3.6 to 0.2 eV with respect to E_F. The red solid square is showing the region selected for high resolution images. (b) Photoemission spectra taken in the A and B region in (a). (c) Angle-integrated valence band photoemission (PES) of $Eu_3F_4Bi_2S_4$. The inset shows the fine images of photoelectron spectromicroscopy in $Eu_3F_4Bi_2S_4$ [the spatial region is depicted as a solid box in (a)], the three images are taken at different energies and shown as shaded regions underneath the PES spectrum.

out within 12 h after cleavage and temperature was kept constant at 40 K during all the measurements.

The normalized Eu L_3-edge XAS spectrum of $Eu_3F_4Bi_2S_4$ is shown in Fig. 1(b). Standard normalization procedure is used that consists of linear fitting of the XAS data in the post-edge region [16]. The observed strong white line peak is related to the Eu $2p_{3/2} \rightarrow 5d$ transition mixed with Eu $4f$ electronic states. When Eu ions show multiple valence, the XAS spectrum is composed of two well separated peaks, representing $4f^7$ and $4f^6$ electronic configuration for Eu. In particular, the lower energy peak at ~6975 eV is due to Eu^{2+} ($4f^7$) state while the peak located at ~6983 eV is due to Eu^{3+} ($4f^6$) state. The presence of the two peaks indicates that the Eu in $Eu_3F_4Bi_2S_4$ is in mixed valence state. The relative intensity of the two peaks can be used to have direct estimation of the average valence. To quantify the average valence, we have decomposed the normalized XAS spectrum into two sets of Lorentzian function and arctangent background. Full width at half-maximum (FWHM) of the Lorentzians is kept the same for both valence states. The energy shift between the two subspectra is kept fixed to 8.2 eV, in accordance with previous literature on valence fluctuating Eu compounds [17]. The best fit curve is shown in Fig. 1(b) using a solid line. The two Lorentzian components are shown below, and the total background (sum of the two background functions) is shown by a dashed line. We obtain the average valence to be 2.20 ± 0.02.

In the previous Mössbauer study by Zhai *et al.*, a static nature is suggested for Eu multiple valence where Eu $4f$ are proposed to be mixed with Bi $6p$ states in the conduction band. They argued that the Eu(1) site is in +2 valence state while Eu(2) is showing mixed valence with an average of +2.6 [8] where the Eu(1) and Eu(2) are shown in Fig. 1(a). In such a scenario the overall valence state would be exactly +2.2, consistent with the present measurements. In this case, the expected doping is about 0.3 electrons per Bi site since in the $Eu_3F_4Bi_2S_4$ the total excess charge is 0.6 electrons (0.2 excess electrons per Eu, and there are three Eu atoms in the $Eu_3F_4Bi_2S_4$) and the total number of Bi atoms in the $Eu_3F_4Bi_2S_4$ is two.

Having demonstrated that Eu in $Eu_3F_4Bi_2S_4$ is in mixed valence with coexisting Eu^{2+} and Eu^{3+} states, however, it cannot be determined if the Eu mixed valence state is intrinsic or it is due to some chemical segregation. In order to address this issue and determine the electronic structure, we have performed space-resolved ARPES, also known as photoelectron spectromicroscopy.

Figure 2(a) shows the spectromicroscopy image of $Eu_3F_4Bi_2S_4$ single crystal right after cleaving, and the colorscale represents the photoelectron intensity integrated between -3.6 and +0.2 eV with respect to the Fermi level (E_F). The sample shows some steps due to nonperfect cleaving, however one can clearly see a large region of homogeneous

photoemission intensity as well. This clarifies that there is no microscale phase separation of any kind in the studied system. We have measured photoemission spectra in the dark (lower intensity) and bright (higher intensity) regions denoted by A and B in Fig. 2(a), respectively, and corresponding photoemission spectra are shown in Fig. 2(b). By comparison, we observe that the spectra in the range of $-2.5 \leqslant E \leqslant 0$ eV are the same while the structure around 3 eV taken at B region is more intense.

Here the cleavage of $Eu_3F_4Bi_2S_4$ is likely to occur in BiS_2 layers. The structure around -3 eV is mainly originated from the S $3p$ orbitals. The presence of such an increased contribution of sulfur states in the region close to the edges of cleavage plane indicates that some defects or reconstruction on the sample surface may exist. Thus we consider that the A region is more appropriate than the B region for a detailed study to determine intrinsic features of the electronic structure. Figure 2(c) shows a typical angle-integrated photoemission spectrum of $Eu_3F_4Bi_2S_4$ measured in the A region. The structure centered at -1.8 eV is composed of Eu^{2+} $4f$ orbitals while the wide double-dome structure between -8 and -10 eV is coming from Eu^{3+} $4f$ multiplet structure. Therefore, it is clear that Eu is indeed in the mixed valence state in this system with coexisting Eu^{2+} and Eu^{3+} states. We have further confirmed that Bi, Eu^{3+}, and Eu^{2+} were indeed distributed homogeneously as follows. Insets of Fig. 2(c) show a fine image of $\sim 80 \times 80$ μm^2 with a pixel size of 1×1 μm^2 taken in the region highlighted by a solid box in Fig. 2(a). These three images are collected at different energy ranges, shown as a shaded area below the photoemission spectrum in Fig. 2(c). We choose three representative energies: the Bi $5d_{5/2}$ core level, the Eu $4f^6$ (Eu^{3+}), and $4f^7$ (Eu^{2+}) levels, and they are labeled as (1), (2), and (3) in Fig. 2(c), respectively. These three images are basically uniform and the small differences are due to difference in counting statistics. By taking maps at Eu^{3+} and Eu^{2+} levels, we clearly observe that no heterogeneity is present in the sample. Therefore, the mixed valence state is not due to nonuniformity or phase separation within the sample, at least in the 1 μm^2 spatial scale. Then we have measured the Fermi surfaces and valence band dispersions inside the boxed region depicted in Fig. 2(a).

The Fermi surface map measured with 74 eV photon energy at 40 K is presented in Fig. 3(a). The photoemission intensity of $Eu_3F_4Bi_2S_4$ at E_F is much weaker compared with other ARPES studies on BiS_2 systems while it becomes comparable around $E = -0.17$ eV. The photoemission intensity map at $E = -0.17$ eV is shown in Fig. 3(b), and one can more clearly see the typical electron pocket around X point than the map at $E = 0.0$ [Fig. 3(a)]. Both maps were integrated within ± 80 meV. The topology of the Fermi surfaces is the same as the RE(O,F)BiS_2 and RE(O,F)$BiSe_2$ systems [6,18,19], indicating that the part of electrons in Eu was introduced to the Bi $6p_x/6p_y$ orbitals. The weak intensity around $-0.17 < E < 0$ eV ($=E_F$) may be related to the existence of structural instability in a tetragonal BiS_2 layer [10,11,20,21]. In fact, local disorder and/or the local structural change [9,22,23] may reduce the lattice symmetry smearing out the electronic features at E_F. Figures 3(c) and 3(d) show the band dispersion near E_F along cut1 and cut2 [see Fig. 3(b)], respectively. Since the intensity at E_F is very weak, it is difficult to determine the Fermi wave

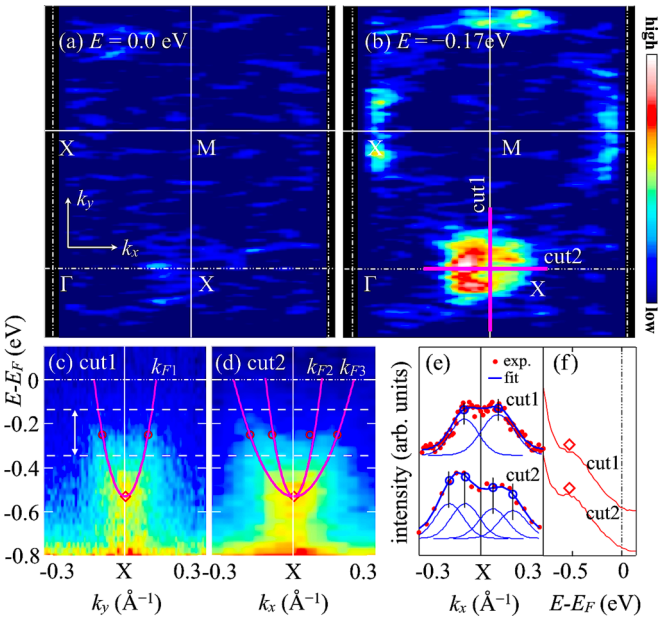

FIG. 3. (a) Fermi surface map and (b) photoemission intensity map at $E = -0.17$ eV of $Eu_3F_4Bi_2S_4$ taken at $h\nu = 74$ eV photons. Both maps were obtained by integrating the spectra in the range of ± 80 meV. Band dispersion near E_F of (c) cut1 and (d) cut2 indicated in (b). (e) MDCs of cut1 and cut2, obtained by integrating $E = -0.25 \pm 0.1$ eV as depicted in (c) and (d). Peak positions were extracted using two Gaussians for cut1 and four Gaussians for cut2. Fit results are also shown, and the peak positions were denoted by circles in (c), (d), and (e). (f) EDCs of cut1 and cut2. Peak positions of EDCs were indicated by squares in (c), (d), and (f). Using the peak positions of MDCs and EDCs, electronlike bands were determined by the fit using quadratic functions depicted in (c) and (d).

numbers. Instead, we use the clearly visible peak positions of momentum distribution curves (MDCs) at $E = -0.25$ eV and energy distribution curves (EDCs), and interpolated quadratic functions in order to estimate the Fermi wave numbers. The MDCs of cut1 and cut2 integrated within $E = -0.25 \pm 0.1$ eV [integrated region is indicated by dashed lines in Figs. 3(c) and 3(d)] are shown in Fig. 3(e), and the peak positions were extracted using two and four Gaussians, respectively, since it is known that the electronlike bands in the X-M direction (cut1) are degenerate while those in the Γ-X direction (cut2) are split into two electronlike bands due to bilayer coupling and/or spin-orbit interaction [5,24]. The Gaussian was selected as a fitting function due to the fact that the present system is characterized by large atomic disorder [9–11] and hence the MDC width may have rather Gaussian character. The experimental data and fit results are, respectively, denoted by solid circles and solid lines in Fig. 3(e). The EDCs integrated within $k = \pm 0.3$ Å^{-1} of cut1 and cut2 are shown in Fig. 3(f), and the peak position (band bottom) can be determined as $E = -0.53$ eV denoted by squares. As a consequence of the determined Fermi wave vectors [$k_{F1} = 0.11 \pm 0.003$ Å^{-1}, $k_{F2} = 0.10 \pm 0.004$ Å^{-1}, $k_{F3} = 0.22 \pm 0.003$ Å^{-1}, see Figs. 3(c) and 3(d)] by the fit on electronlike bands, Luttinger theorem allows us to estimate the effective carrier concentration as 0.23 ± 0.01 electrons per Bi site in $Eu_3F_4Bi_2S_4$, where the inner and outer Fermi surfaces,

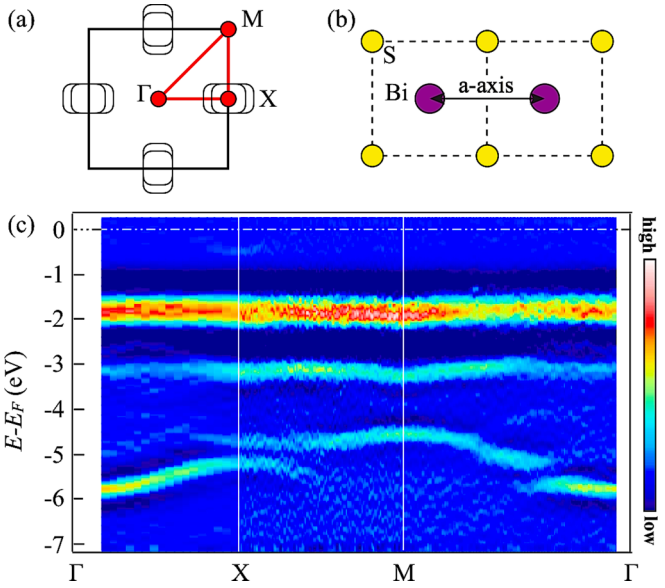

FIG. 4. (a) Schematic diagram of the Fermi surfaces and Brillouin zone. (b) A sketch of the atomic arrangement in the BiS_2 layer with tetragonal symmetry. (c) ARPES spectra (second derivative in the energy direction) measured along the high symmetry lines of the Brillouin zone as depicted in (a).

respectively, enclose $3.6 \pm 0.24\%$ and $8.0 \pm 0.30\%$ of the Brillouin zone. From this estimation, one can also classify that the $Eu_3F_4Bi_2S_4$ system is in the underdoped region of the phase diagram. The difference between the value estimated by XAS (0.3) and by ARPES (0.23) can be related to the Bi defects reported by scanning tunneling microscope study [25] and/or part of electrons were trapped in interstitial sites induced by strong local atomic disorder, one of the common features in BiS_2-based systems [9,23]. Having confirmed that the present $Eu_3F_4Bi_2F_4$ material is a self-doped system, it is worth pointing out the pressure dependence of the conductivity (as well as T_c) that changes monotonically with increasing pressure up to ~2.26 GPa [26]. This indicates that carrier concentration can be controlled by pressure and the average Eu valence may also involve accordingly with increasing pressure, and Fermi surface topology may change due to the extra self-doped electrons.

The valence band dispersion was taken along high symmetry Γ-X-M lines of the squared Brillouin zone [$(2\pi/a)\text{Å}^{-1} \times (2\pi/a)\text{Å}^{-1}$] as depicted in Fig. 4(a) where a is defined by Bi-Bi distance in Fig. 4(b). The valence band dispersion is shown in Fig. 4(c). Besides the electron pockets around X point, a strong nondispersive band coming from Eu $4f$ orbitals is clearly visible at around -1.8 eV. Below the Eu $4f$ flat band, we observed several bands, and they are most likely from F $2p$ and S $3p$ contributions. The existence of Eu $4f$ flat band just below the electronlike pockets is similar to the $CeO_{1-x}F_xBiS_2$ system, where the Ce $4f$ flat band exists just below the electronlike pockets [27]. In the $CeO_{1-x}F_xBiS_2$ system, the Ce $4f$ electrons are found to be in a well-localized state [28]. Even though the lattice structure of the block layer and *RE* are different, similar physics is likely to describe the physics of the $Eu_3F_4Bi_2S_4$ system as well.

In summary, we have studied the electronic structure of the self-doped $Eu_3F_4Bi_2S_4$ system using a combination of Eu L_3-edge XAS and space-resolved ARPES. From the Eu L_3-edge XAS measurement, we have observed that the Eu valence state is a Eu^{2+}/Eu^{3+} mixed valence state that is consistent with the photoemission results. We have estimated that 0.3 excess electrons exist per Bi site in $Eu_3F_4Bi_2S_4$. From the space-resolved ARPES, we have ruled out any possibility of microscale phase separation in the system. The Fermi surfaces and band structures were similar to other BiS_2-based compounds showing disconnected rectangular electronlike pockets around the X point. Luttinger volume analysis on the Fermi surfaces suggests that the effective carrier concentration is 0.23 electrons per Bi site, and this system is still in the underdoped region of its phase diagram. Moreover, we observed that the photoemission intensity near E_F is found to be weak. We propose this effect to be related to disorder at the atomic level.

T.S. acknowledges the support from JSPS Research Fellowship for Young Scientists. This work is part of the bilateral agreements of Sapienza - University of Tokyo, Sapienza - Tokyo Metropolitan University, and Sapienza - Okayama University. This research was partially supported by the Program for Promoting the Enhancement of Research Universities from MEXT and the Program for Advancing Strategic International Networks to Accelerate the Circulation of Talented Researchers from JSPS. The work at Sapienza is partially supported by PRIN2012 (Grant No. 2012X3YFZ2) of MIUR, Italy. Part of this work was supported by JSPS KAKENHI (Grant No. 15H03693, 15H05884).

[1] Y. Mizuguchi, H. Fujihisa, Y. Gotoh, K. Suzuki, H. Usui, K. Kuroki, S. Demura, Y. Takano, H. Izawa, and O. Miura, Phys. Rev. B **86**, 220510 (2012).

[2] Y. Mizuguchi, S. Demura, K. Deguchi, Y. Takano, H. Fujihisa, Y. Gotoh, H. Izawa, and O. Miura, J. Phys. Soc. Jpn. **81**, 114725 (2012).

[3] D. Yazici, K. Huang, B. D. White, I. Jeon, V. W. Burnett, A. J. Friedman, I. K. Lum, M. Nallaiyan, S. Spagna, and M. B. Maple, Phys. Rev. B **87**, 174512 (2013).

[4] H. Kotegawa, Y. Tomita, H. Tou, H. Izawa, Y. Mizuguchi, O. Miura, S. Demura, K. Deguchi, and Y. Takano, J. Phys. Soc. Jpn. **81**, 103702 (2012).

[5] H. Usui, K. Suzuki, and K. Kuroki, Phys. Rev. B **86**, 220501 (2012).

[6] T. Sugimoto, D. Ootsuki, C. Morice, E. Artacho, S. S. Saxena, E. F. Schwier, M. Zheng, Y. Kojima, H. Iwasawa, K. Shimada, M. Arita, H. Namatame, M. Taniguchi, M. Takahashi, N. L. Saini, T. Asano, R. Higashinaka, T. D. Matsuda, Y. Aoki, and T. Mizokawa, Phys. Rev. B **92**, 041113(R) (2015).

[7] H.-F. Zhai, Z.-T. Tang, H. Jiang, K. Xu, K. Zhang, P. Zhang, J.-K. Bao, Y.-L. Sun, W.-H. Jiao, I. Nowik, I. Felner, Y.-K. Li, X.-F. Xu, Q. Tao, C.-M. Feng, Z.-A. Xu, and G.-H. Cao, Phys. Rev. B **90**, 064518 (2014).

[8] H.-F. Zhai, P. Zhang, S.-Q. Wu, C.-Y. He, Z.-T. Tang, H. Jiang, Y.-L. Sun, J.-K. Bao, I. Nowik, I. Felner, Y.-W. Zeng, Y.-K. Li, X.-F. Xu, Q. Tao, Z.-A. Xu, and G.-H. Cao, J. Am. Chem. Soc. **136**, 15386 (2014).

[9] E. Paris, B. Joseph, A. Iadecola, T. Sugimoto, L. Olivi, S. Demura, Y. Mizuguchi, Y. Takano, T. Mizokawa, and N. L. Saini, J. Phys.: Condens. Matter **26**, 435701 (2014).

[10] Q. Liu, X. Zhang, and A. Zunger, Phys. Rev. B **93**, 174119 (2016).

[11] X. Zhou, Q. Liu, J. A. Waugh, H. Li, T. Nummy, X. Zhang, X. Zhu, G. Cao, A. Zunger, and D. S. Dessau, arXiv:1607.02796.

[12] J. Kajitani, H. Endo, M. Mita, R. Higashinaka, T. D. Matsuda, and Y. Aoki (unpublished).

[13] O. Proux, V. Nassif, A. Prat, O. Ulrich, E. Lahera, X. Biquard, J.-J. Menthonnex, and J.-L. Hazemann, J. Synchrotron Rad. **13**, 59 (2006).

[14] B. Ravel and M. Newville, J. Synchrotron Rad. **12**, 537 (2005).

[15] P. Dudin, P. Lacovig, C. Fava, E. Nicolini, A. Bianco, G. Cautero, and A. Barinov, J. Synchrotron Rad. **17**, 445 (2010).

[16] G. Bunker, *Introduction to XAFS* (Cambridge University Press, Cambridge, 2010), Sec. 5, p. 146.

[17] H. J. Hesse, R. Lubbers, M. Winzenick, H. W. Neuling, and G. Wortmann, J. Alloys Compd. **246**, 220 (1997).

[18] K. Terashima, J. Sonoyama, T. Wakita, M. Sunagawa, K. Ono, H. Kumigashira, T. Muro, M. Nagao, S. Watauchi, I. Tanaka, H. Okazaki, Y. Takano, O. Miura, Y. Mizuguchi, H. Usui, K. Suzuki, K. Kuroki, Y. Muraoka, and T. Yokoya, Phys. Rev. B **90**, 220512 (2014).

[19] N. L. Saini, D. Ootsuki, E. Paris, B. Joseph, A. Barinov, M. Tanaka, Y. Takano, and T. Mizokawa, Phys. Rev. B **90**, 214517 (2014).

[20] T. Yildirim, Phys. Rev. B **87**, 020506(R) (2013).

[21] A. Athauda, J. Yang, S. Lee, Y. Mizuguchi, K. Deguchi, Y. Takano, O. Miura, and D. Louca, Phys. Rev. B **91**, 144112 (2015).

[22] T. Sugimoto, B. Joseph, E. Paris, A. Iadecola, T. Mizokawa, S. Demura, Y. Mizuguchi, Y. Takano, and N. L. Saini, Phys. Rev. B **89**, 201117(R) (2014).

[23] Y. Mizuguchi, E. Paris, T. Sugimoto, A. Iadecola, J. Kajitani, O. Miura, T. Mizokawa, and N. L. Saini, Phys. Chem. Chem. Phys. **17**, 22090 (2015).

[24] L. K. Zeng, X. B. Wang, J. Ma, P. Richard, S. M. Nie, H. M. Weng, N. L. Wang, Z. Wang, T. Qian, and H. Ding, Phys. Rev. B **90**, 054512 (2014).

[25] T. Machida, Y. Fujisawa, M. Nagao, S. Demura, K. Deguchi, Y. Mizuguchi, Y. Takano, and H. Sakata, J. Phys. Soc. Jpn. **83**, 113701 (2014).

[26] Y. Luo, H.-F. Zhai, P. Zhang, Z.-A. Xu, G.-H. Cao, and J. D. Thompson, Phys. Rev. B **90**, 220510 (2014).

[27] T. Sugimoto, D. Ootsuki, E. Paris, A. Iadecola, M. Salome, E. F. Schwier, H. Iwasawa, K. Shimada, T. Asano, R. Higashinaka, T. D. Matsuda, Y. Aoki, N. L. Saini, and T. Mizokawa, Phys. Rev. B **94**, 081106(R) (2016).

[28] R. Higashinaka, T. Asano, T. Nakashima, K. Fushiya, Y. Mizuguchi, O. Miura, T. D. Matsuda, and Y. Aoki, J. Phys. Soc. Jpn. **84**, 023702 (2015).